Experimental signatures of emergent quantum electrodynamics in a quantum spin ice

Romain Sibille[1,2], Nicolas Gauthier[2], Han Yan[3], Monica Ciomaga Hatnean[4], Jacques Ollivier[5], Barry Winn[6], Geetha Balakrishnan[4], Michel Kenzelmann[2,1], Nic Shannon[3] & Tom Fennell[1]

[1]Laboratory for Neutron Scattering and Imaging, Paul Scherrer Institut, 5232 Villigen PSI, Switzerland, [2]Laboratory for Scientific Developments and Novel Materials, Paul Scherrer Institut, 5232 Villigen PSI, Switzerland, [3]Okinawa Institute of Science and Technology Graduate University, Onna-son, Okinawa 904-0495, Japan, [4]Physics Department, University of Warwick, Coventry, CV4 7AL, UK, [5]Institut Laue-Langevin, CS 20156, F-38042 Grenoble Cedex 9, France, [6]Quantum Condensed Matter Division, Oak Ridge National Laboratory, Oak Ridge, Tennessee, USA, [*]email: romain.sibille@psi.ch

In a quantum spin liquid, the magnetic moments of the constituent electron spins evade classical long-range order to form an exotic state that is quantum entangled and coherent over macroscopic length scales[1-2]. Such phases offer promising perspectives for device applications in quantum information technologies, and their study can reveal fundamentally novel physics in quantum matter. *Quantum spin ice* is an appealing proposal of one such state, in which a quantum field theory describes the fundamental ground state properties and excitations[3-6]. An emergent *U*(1) gauge structure endows this quantum-coherent regime with quasiparticles that are predicted to behave like magnetic and electric monopoles, along with a gauge boson playing the role of an artificial photon. However, this emergent lattice quantum electrodynamics has not yet been observed experimentally. Here we report neutron scattering measurements of the rare-earth pyrochlore magnet $Pr_2Hf_2O_7$ that provide evidence for a *quantum spin ice* ground state. We find a quasielastic structure factor with pinch points – a signature of a classical spin ice – that are partially suppressed, as expected in the quantum-coherent regime of the lattice field theory at finite temperature. Our result allows an estimate for the speed of light associated with magnetic photon excitations. We also reveal a continuum of inelastic spin excitations, a property of the fractionalized excitations defining quantum spin liquids, which relate to the monopole excitations of the gauge theory. Our results constitute an experimental discovery of a condensed matter system whose low-energy physics can be described by emergent quantum electrodynamics. The observation of a *quantum spin ice* ground state provides a concrete example of a three-dimensional quantum spin liquid, a topical state of matter, which so far has only been reported in lower dimensionalities.

The idea of a spin system that lacks symmetry-breaking magnetic order at zero temperature but develops quantum entanglement traces back to 1973 Anderson's proposal in which valence bonds between neighboring spins pair into singlets and resonate on the lattice[7]. The idea was then extended to valence bonds at all length scales, leading to a macroscopically quantum entangled ground state wave-function and a quantum spin liquid (QSL)[1-2]. Models to construct highly-entangled QSLs have been developed for various low-dimensional and/or frustrated model systems[1-2,8-9]. An exciting aspect is the emergence of exotic excitations carried by such phases, which behave as quasiparticles and can only be produced by an infinite product of local operators – a direct consequence of the many-body entanglement. For instance, the excitations of antiferromagnetic spin-half (S = 1/2) chains are deconfined spinons, each carrying S = 1/2 – fractionalized quasiparticles that are fundamentally different to the S = 1 magnons of conventional three-dimensionally ordered magnets. They have been measured as continua of spin excitations in neutron scattering experiments on one-dimensional magnets such as $KCuF_3$[10]. The physics of fractionalization is also visible in two-dimensional magnets, e.g. kagome-lattice $ZnCu_3(OD)_2Cl_2$[11], honeycomb-lattice α-$RuCl_3$[12] and triangular-lattice $YbMgGaO_4$[13]. However, the experimental evidence for a QSL state stabilized in three dimensions is still absent and the signatures of QSL states that allow direct comparison with theoretical models remain rather elusive.

In three dimensions, spin ice[14,15] is a well-established paradigm to stabilize *classical* spin liquids. In rare-earth pyrochlore materials such as $Ho_2Ti_2O_7$, Ising-like magnetic moments decorate a lattice of corner-sharing tetrahedra. A local constraint – the 2-in-2-out 'ice rule' acting on each tetrahedron – leads to a manifold of degenerate ground states where the spin correlations create an emergent gauge field, $\mathcal{A}(\boldsymbol{r})$ in real space. The ice rule endows the gauge field with a zero-divergence condition that can be written $\mathcal{B}(\boldsymbol{r}) = \nabla \times \mathcal{A}(r)$, where $\mathcal{B}(\boldsymbol{r})$ has the physical meaning of the local magnetization. The result is a Coulomb phase[16,17] where spin flips violating the ice rule generate magnetic monopoles[18], a mobile magnetic charge regarded as a quasiparticle carrying half of the dipole moment, which interact by emergent classical magnetostatics. Specific signatures of the emergent gauge symmetry appear in neutron scattering experiments on spin ices, in which the diffuse response typical of spin liquids acquires pinch points at specific wave-vectors[16,17]. Currently, the quantum spin ice (QSI) state forms a formidable challenge[6]. This type of QSL is a generalization of the classical spin ice that includes quantum fluctuations, whose effective field theory becomes emergent quantum electrodynamics[3,4]. Time fluctuations of the gauge field $\mathcal{A}(\boldsymbol{r})$ give rise to an electric field, $\mathcal{E}(\boldsymbol{r})$, and the ground state is governed by the Maxwell equation

$$\mathcal{S}_{Maxwell} = \frac{1}{8\pi} \int dt d^3\boldsymbol{r} \, [\mathcal{E}(\boldsymbol{r})^2 - c^2 \mathcal{B}(\boldsymbol{r})^2],$$

which supports linearly dispersing transverse excitations of the gauge field, i.e. emergent photons with a speed of light *c*. The gauge theory of the QSI also supports gapped excitations, which are magnetic monopoles – akin to spinons – and electric monopoles, all described as quantum coherent quasiparticles.

Formally, the QSI can be constructed by introducing transverse terms into an effective *S* = 1/2 Hamiltonian on the pyrochlore lattice[19,20], so that fluctuations between the degenerate ice rule states become allowed via quantum tunneling[3-6]. It was proposed that, in praseodymium-based pyrochlore materials, multipolar couplings can introduce effective transverse exchange couplings between the low-energy effective *S* = 1/2 moments[21]. Experimental investigations on $Pr_2Zr_2O_7$ conform to this theoretical proposal[22], but the results appear affected by structural disorder that brings additional effects into play[23,24]. Recently, another QSI candidate, $Pr_2Hf_2O_7$, has emerged as a clean realization of a system of Pr^{3+} Ising-like moments interacting on a perfect pyrochlore lattice[25]. We have produced large high-quality single crystals of $Pr_2Hf_2O_7$, by optimizing the conditions of the traveling solvent floating zone growth so that, despite the high melting temperature of about 2400 Celsius, the evaporation of praseodymium during this process is reduced as much as practically possible. As a result, the structural and magnetic properties are identical for our powder and single crystal samples, and there is no evidence for any sort of defects compared to a perfect cubic pyrochlore structure.

In $Pr_2Hf_2O_7$, a sizeable crystal field gap, about 9 meV ~ 100 K, isolates a non-Kramers ground doublet with magnetic moment of ~ 2.4 μ_B[25]. Temperatures much lower than the gap allow the description of the magnetic properties by an effective *S* = 1/2 local moment. The wave-function of this single-ion ground state doublet[25] leads to a strong Ising anisotropy at low temperature, as needed to stabilize a spin ice, and incorporates quadrupolar terms, which make it possible for the spin ice to acquire quantum dynamics through transverse exchange. Interestingly, the material displays no indication of symmetry-breaking order down to at least 0.05 K. However, a cooperative regime develops below 0.5 K, with macroscopic indications of spin ice correlations[25]. We present inelastic neutron scattering (INS) measurements, at approximately 0.05 K on our single crystals of $Pr_2Hf_2O_7$, in order to study the energy–momentum (*E*–***k***) dependence of the signals characterizing the correlated regime.

An overview of our data measured with unpolarized neutrons of incident energy E_i = 2.7 meV is presented in Fig. 1, which shows constant-energy maps of the (H,H,L) plane in reciprocal space. Data on Fig. 1**a** were integrated around E = 0 ± 0.06 meV after subtraction of a background dataset measured at 50 K. The subtraction provides a good estimate of the magnetic part of the elastic structure factor at 0.05 K, which is directly proportional to the spin–spin correlation function. Bragg peaks that would indicate long-range magnetic order remain absent, but we observe a pattern of diffuse scattering that is characteristic of a spin liquid[1]. The magnetic nature of this elastic signal was confirmed using polarized INS, as shown by the spectrum presented on Fig. 2**a**, where the spin flip scattering of neutrons polarized in the horizontal plane (X-SF) is a purely magnetic signal[16]. Our elastic structure factor of $Pr_2Hf_2O_7$ (Fig. 1**a**) has the general shape observed in pyrochlore materials with spin ice correlations, i.e. pinch points appear at Brillouin zone centers (0,0,2) and (1,1,1), extending into more diffuse scattering around wave-vectors **k** such as (0,0,3) and (3/2,3/2,3/2)[15].

In Fig. 3 we plot the result of elastic cuts through the pinch point wave-vector (0,0,2), along the solid black lines shown in Fig. 1**a**, in order to diagnose the nature of the spin ice correlations in $Pr_2Hf_2O_7$. Our experiment indicates that pinch points appear in unpolarized scattering, which is in striking contrast to classical dipolar spin ices such as $Ho_2Ti_2O_7$ where these features are only visible in the spin flip scattering of polarized neutrons. Our observation suggests that, as expected due to the smaller magnetic moments, $Pr_2Hf_2O_7$ rather conforms to a near-neighbor spin ice model where pinch points are expected to be found in unpolarized neutron scattering (see the results of analytical calculations for a classical near-neighbor spin ice – red dashed lines in Fig. 3)[16]. However, pinch-point features in $Pr_2Hf_2O_7$ appear to be suppressed relative to the classical spin ice model. Pinch-point scattering can be suppressed by quantum fluctuations[26], and therefore we test this hypothesis by comparing the data with the predictions of a lattice field theory of a QSI[5]. The calculation of the equal-time QSI structure factor within the integration ranges of our experiment (Fig. 1**b**) compares favorably with our data (Fig. 1**a**), with minor differences that we attribute to non-universal characteristics of $Pr_2Hf_2O_7$. Meanwhile, the two cuts shown in Fig. 3 reveal that both the experimental data (points with error bars), and the theoretical prediction for a QSI (blue solid line), show clear deviations from the predictions of a classical spin ice. The best quantitative fits to the data are obtained using the QSI model for a temperature $T/ca_0^{-1} = 1.8 \pm 0.1$ (a_0 being the lattice constant of the pyrochlore cubic unit cell), which translates into a speed of light $c \approx 3.6\ m/s$ for the artificial photons (assuming T = 0.05 K). Such photon quasiparticles would appear in INS as gapless excitations with a bandwidth $\Delta E \approx 0.01$ meV, so that any photon spectral weight is integrated in our results of

elastic scattering. This is consistent with the absence of low-lying dispersive excitations in the inelastic scattering (see below).

Energy spectra taken in our INS data measured with unpolarized neutrons are shown on Fig. 2**b**, providing evidence for two major contributions to the inelastic response of the sample at 0.05 K. The dominant contribution is an excitation centered around E = 0.2 meV (consistent with our data taken on a powder sample at the same temperature[25]), whose structure factor is presented on Fig. 1**c**. Secondly, we identify a continuum of spin excitations that extends up to at least E = 1 meV, and whose spectral intensity is also broadly distributed in momentum. We note that these inelastic signals are magnetic, as demonstrated by the polarized INS data on Fig. 2**a**, and that they become part of the quasielastic spectrum when the temperature is raised above 0.5 K.

A gapped continuum of spin excitations is expected from the magnetic monopoles propagating via quantum tunneling – or spinons – that characterize a QSI[3-6]. Our results appear consistent with recent theoretical work where spinons were found to propagate as massive, nearly free quantum particles as a result of their coupling to a background of disordered spin-ice configurations[27]. The bandwidth of the spinon excitations in $Pr_2Hf_2O_7$ is one order of magnitude higher than the effective exchange interaction, $J \approx 1.2$ K ≈ 0.1 meV, which also appears consistent with theoretical predictions[27-29]. The form of scattering found at finite energy (Fig. 1**c**) is also highly reminiscent of quantum Monte Carlo simulations results for QSI at temperatures where there is a finite density of spinons[30]. It is interesting to contrast this behavior with that of $Pr_2Zr_2O_7$, where correlations reminiscent of spin ice have also been observed in inelastic neutron scattering experiments, but above an energy gap of $E \approx 0.3$ meV[22,23]. These dynamical spin-ice correlations can be interpreted as excitations out of a ground state in which the quadrupolar component of the Pr^{3+} ion is ordered[23]. It seems less likely that this scenario applies to $Pr_2Hf_2O_7$, where (suppressed) pinch points are found in quasi-elastic scattering, and not at finite energy.

Our results suggest that $Pr_2Hf_2O_7$ adopts a QSI ground state with fractionalized excitations – an important type of three-dimensional QSL. Our experimentally observed correlations display a striking match to the predictions of a compact $U(1)$ gauge theory. We have measured the suppressed pinch points expected in the quantum coherent regime with emergent photons, and the continuum of excitations expected from the existence of spinons, together making a strong case that $Pr_2Hf_2O_7$ is a QSI. While our experimental observation is an important breakthrough, we believe that it will motivate further works on this material. There are further experimental challenges to fully characterize the QSI state, such as measuring the expected T^3 heat capacity

associated with the linearly dispersing photons at low temperature[3,5] and determining the entropy associated with the spin liquid state, which is a fundamental question in the context of the third law of thermodynamics; determining how pinch points are suppressed as a function of temperature[5], which provides important information about quantum coherence in the QSI state; or directly probing the photons using high resolution techniques. On the theory side, predictions are needed concerning the structure factor of the spinons and a possible coexistence of the QSI with quadrupolar correlations. These developments would pave the way for exploring the possibilities of a genuine QSL.

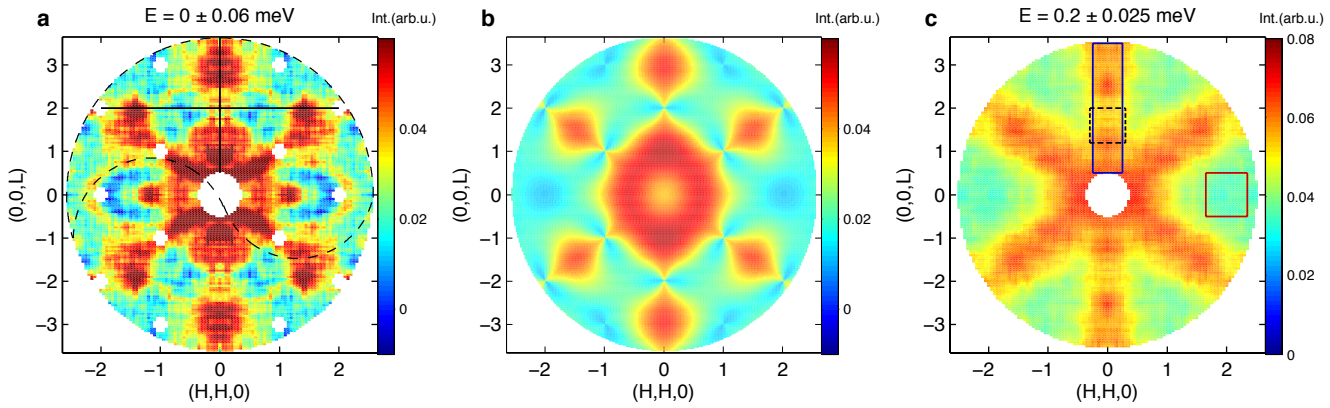

Figure 1 | Momentum dependence of the magnetic correlations (a-b) and magnetic excitations (c) in $Pr_2Hf_2O_7$. We show two-dimensional cuts in the (H,H,L) plane of reciprocal space, integrated around two different values of energy transfer. Data were collected using time-of-flight (ToF) inelastic neutron scattering (INS) at a temperature of 0.05 K on the IN5 instrument (unpolarized neutrons). The incident neutron energy was fixed to E_i = 2.70 meV, providing an energy resolution at zero energy transfer of 0.05 meV (full width at half maximum). Data were measured in the upper quadrant shown by the black dashed curves on panel **a**, corrected for sample absorption and electronic noise, and then symmetrized (Methods). Maps shown on panels **a-c** are integrated over a thin range of momentum transfer, (H,-H,0) ± 0.05 r.l.u., in the direction perpendicular to the (H,H,L) plane. Panel **a** shows data that were integrated around zero-energy transfer (E = 0 ± 0.06 meV) after subtraction of a background dataset measured with the same statistics at a temperature of 50 K (all other conditions remaining unchanged). We refer to the data of panel **a** as 'elastic data', which, in our interpretation, mainly reflects the equal-time spin correlations of the quantum spin ice (QSI), including contributions from low-energy gapless photon excitations. The two continuous black lines in panel **a**, crossing each other at the wave-vector (0,0,2) where pinch point scattering is suppressed in a QSI, indicate the directions of the momentum dependent cuts shown on Fig. 3. Panel **b** shows the results calculated using the lattice field theory of the QSI, for comparison with the experimental data of panel **a**. The calculation is done at the finite temperature deduced from the fit shown on Fig. 3. Panel **c** shows inelastic data integrated around a finite value of energy transfer, E = 0.2 ± 0.025 meV. The background is negligible in the inelastic channels at E > 0.1 meV. The blue and red boxes on panel **c** are the integration areas in the data as they are shown here, of the energy spectra shown on Fig. 2**b**. The box delimited by black dashed lines on panel **c** of Fig. 1 represents the integration area that was used to generate the energy spectrum, shown on Fig. 2**a**, through polarized INS data (not shown).

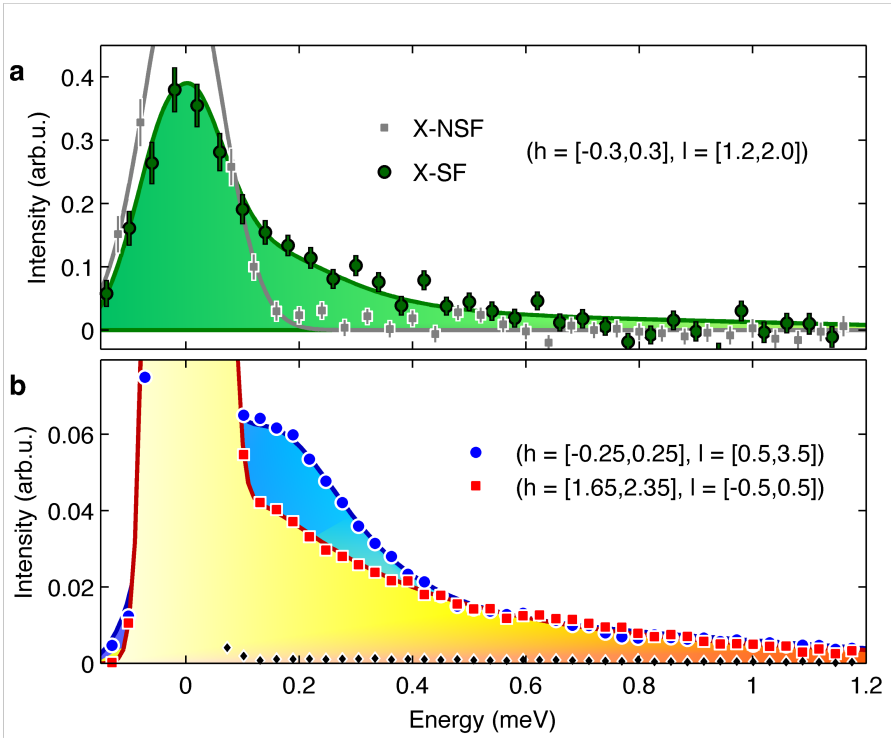

Figure 2 | Energy spectra at fixed positions in momentum space. We present constant-momentum cuts through our time-of-flight (ToF) inelastic neutron scattering (INS) data measured at a temperature of 0.05 K. The integration areas in momentum space are indicated with two vectors, h = [H,H,0] and l = [0,0,L], which correspond to the rectangles drawn on Fig. 1**c**. Data shown on panel **a** result from a polarized INS experiment realized on the instrument HYSPEC. We show the spin flip and non-spin flip scattering measured with neutrons that were polarized in the horizontal plane of the instrument, X-SF and X-SNF, respectively. The X-SF scattering is a purely magnetic signal. The data on panel **a** demonstrate the existence of elastic and inelastic (over the entire range of accessible energy transfers *E*) signals that are, unambiguously, magnetic scattering. On panel **b** we show the energy cuts through the unpolarized INS data measured on IN5 and shown on Fig. 1. The integration in two specific areas of reciprocal space, where the intense inelastic part of the inelastic spectrum centered on *E* = 0.2 meV is either dominant (blue symbols) or negligible (red symbols), evidences a continuum of inelastic scattering attributed to spinon excitations. The black symbols on panel **b** show an energy spectrum through data collected at a temperature of 50 K, scaled by the ratio of the Bose factors at 50 K and 0.05 K, which gives an estimate of the inelastic background at 0.05 K.

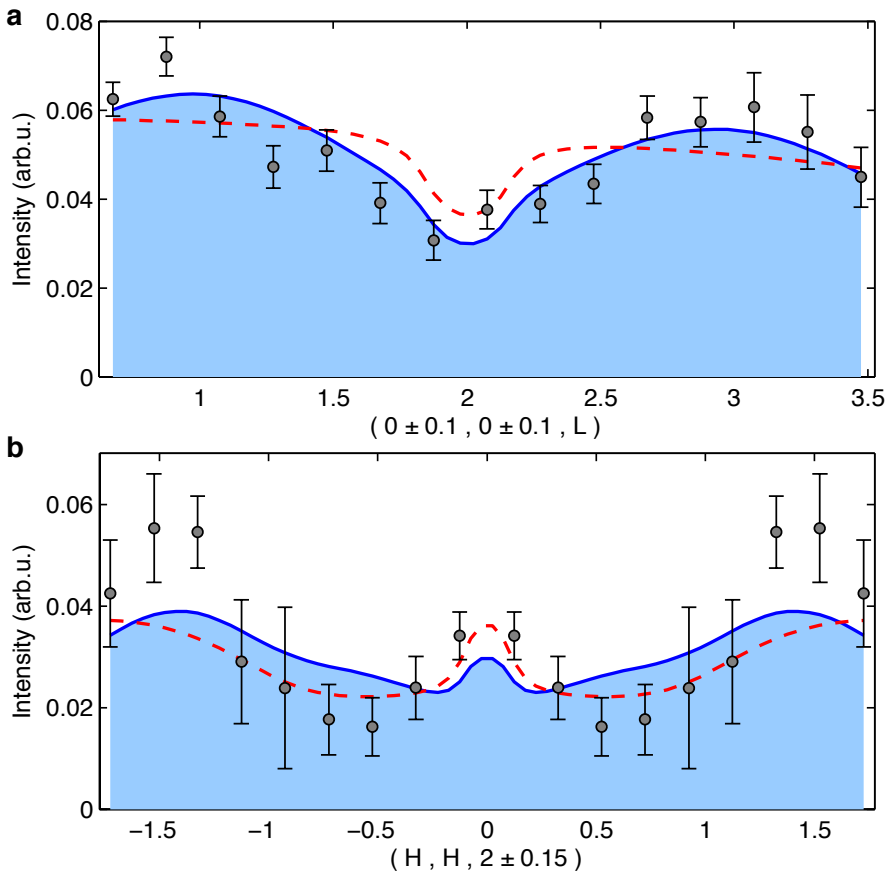

Figure 3 | Line shape of the suppressed pinch points measured in $Pr_2Hf_2O_7$, and comparison with model calculations. The data points with error bars show the results of radial (**a**) and transverse (**b**) cuts through the experimental data shown on Fig. 1**a**. The two cuts, whose directions are shown with black lines on Fig. 1**a**, cross each other at the zone center (0,0,2), where a pinch point is expected to occur. The experimental data are compared with the prediction for both a classical near-neighbor spin ice (red dashed line) and a quantum spin ice[5] (QSI, solid blue line). Finite experimental resolution, modeled through an integration over a finite range of wave-vectors, leads to a small dip in the prediction for a classical spin ice around (0,0,2), visible in the transverse cut **a**, and eliminates a sharp spike at the same wave-vector in the transverse cut **(b).** For the radial cut shown on panel **a**, quantum fluctuations lead to a further suppression of scattering around (0,0,2), as well as an enhancement of scattering around (0,0,1) and (0,0,3). For the transverse cut presented on panel **b**, quantum fluctuations lead to a non-monotonic evolution of scattering between H = 0.5 and H = 2. All of these QSI features are present in the experimental data, and the best fits for both cuts are obtained using a QSI model at a finite temperature $T/ca_0^{-1} = 1.8 \pm 0.1$, where a_0 is the lattice constant of the pyrochlore cubic unit cell and c is the speed of light of emergent photons ($c \approx 3.6\ m/s$ for T = 0.05 K). Further details of models and fits are provided in the "Methods" section.

References

1. Balents, L. Spin liquids in frustrated magnets. *Nature* **464**, 199 (2010).
2. Savary, L & Balents, L. Quantum spin liquids: a review. *Rep. Prog. Phys.* **80**, 016502 (2016).
3. Hermele, M., Fisher, M. P. A. & Balents, L. Pyrochlore photons: The *U*(1) spin liquid in a *S* = ½ three-dimensional frustrated magnet. *Phys. Rev. B* **69**, 064404 (2004).
4. Banerjee, A., Isakov, S. V., Damle, K. & Kim, Y.-B. Unusual Liquid State of Hard-Core Bosons on the Pyrochlore Lattice, *Phys. Rev. Lett.* **100**, 047208 (2008).
5. Benton, O., Sikora, O. & Shannon, N. Seeing the light: Experimental signatures of emergent electromagnetism in a quantum spin ice. *Phys. Rev. B* **86**, 075154 (2012).
6. Gingras, M. J. P. & McClarty, P. A. Quantum spin ice: a search for gapless quantum spin liquids in pyrochlore magnets. *Rep. Prog. Phys.* **77**, 056501 (2014).
7. Anderson, P. W. Resonating valence bonds. *Mat. Res. Bull.* **8**, 153 (1973).
8. Wen, X-G. Quantum orders and symmetric spin liquids. *Phys. Rev. B* **65** 165113 (2002).
9. Moessner, R. and Sondhi, S. L. Resonating valence bond liquid physics on the triangular lattice. *Prog. Theor. Phys.* **145** (Suppl.), 37–42 (2002).
10. Tennant, D. A., Perring, T. G., Cowley, R. A., & Nagler, S. E. Unbound spinons in the spin-1/2 antiferromagnetic chain $KCuF_3$. *Phys. Rev. Lett,* **70** 4003–4006 (1993).
11. Han, T.-H. *et al.* Fractionalized excitations in the spin-liquid state of a kagome-lattice antiferromagnet. *Nature* **492**, 406–410 (2012).
12. Banerjee, A. *et al.* Proximate Kitaev quantum spin liquid behaviour in a honeycomb magnet. *Nature Mater.* **15**, 733–740 (2016).
13. Shen, Y. *et al.* Evidence for a spinon Fermi surface in a triangular-lattice quantum-spin-liquid candidate. *Nature* **540**, 559–562 (2016).
14. Castelnovo, C., Moessner, R. & Sondhi, S. L. Spin Ice, Fractionalization, and Topological Order. *Annu. Rev. Condens. Matter Phys.* **3**, 35–55 (2012).
15. Bramwell, S. T. *et al.* Spin Correlations in $Ho_2Ti_2O_7$: a Dipolar Spin Ice System. *Phys. Rev. Lett.* **87**, 047205 (2001).
16. Fennell, T. *et al.* Magnetic Coulomb Phase in the Spin Ice $Ho_2Ti_2O_7$. *Science* **326**, 415 (2009).
17. Henley, C.L. The “Coulomb Phase” in frustrated systems. *Annu. Rev. Condens. Matter Phys.* **1**, 179-210 (2010).
18. Castelnovo, C., Moessner, R. & Sondhi, S. L. Magnetic monopoles in spin ice. *Nature* **451**, 42–45 (2008).
19. Curnoe, S. H. Structural distortion and the spin liquid state in $Tb_2Ti_2O_7$. *Phys. Rev. B* **78**, 094418 (2008).
20. Ross, K. A., Savary, L., Gaulin, B. D. & Balents, L. Quantum Excitations in Quantum Spin Ice. *Phys. Rev. X* **1**, 021002 (2011).
21. Onoda, S. & Tanaka, Y. Quantum Melting of Spin Ice: Emergent Cooperative Quadrupole and Chirality. *Phys. Rev. Lett.* **105**, 047201 (2010).
22. Kimura, K. *et al.* Quantum fluctuations in spin-ice-like $Pr_2Zr_2O_7$. *Nat Commun* **4**, 1934 (2013).
23. Petit, S. *et al.* Antiferroquadrupolar correlations in the quantum spin ice candidate $Pr_2Zr_2O_7$. *Phys. Rev. B* **94**, 165153 (2016).

24. Wen, J.-J. *et al.* Disordered Route to the Coulomb Quantum Spin Liquid: Random Transverse Fields on Spin Ice in $Pr_2Zr_2O_7$. *Phys. Rev. Lett.* **118**, 107206 (2017).

25. Sibille, R. *et al.* Candidate quantum spin ice in the pyrochlore $Pr_2Hf_2O_7$. *Phys. Rev. B* **94**, 024436 (2016).

26. Shannon, N., Sikora, O., Pollmann, Penc, K. & Fulde, P. Quantum Ice: A Quantum Monte Carlo Study. *Phys. Rev. Lett.* **108**, 067204 (2012).

27. Wan, Y., Carrasquilla, J. & Melko, R. G. Spinon Walk in Quantum Spin Ice. *Phys. Rev. Lett.* **116**, 167202 (2016).

28. Hao, Z., Day, A. G. R. & Gingras, M. J. P. Bosonic many-body theory of quantum spin ice. *Phys. Rev. B* **90**, 214430 (2014).

29. Petrova, O., Moessner, R. & Sondhi, S. L. Hydrogenic states of monopoles in diluted quantum spin ice. *Phys. Rev. B* **92**, 100401(R) (2015).

30. Kato, S. & Onoda, S. Numerical Evidence of Quantum Melting of Spin Ice: Quantum-to-Classical crossover. *Phys. Rev. Lett.* **115**, 077202 (2015).

Acknowledgements

We acknowledge the Institut Laue Langevin, ILL (Grenoble, France, EU) for the allocated beamtime. We acknowledge funding from the Swiss National Science Foundation (Grants No. 200021_140862, Quantum Frustration in Model Magnets; and No. 200021_138018). This research used resources at the Spallation Neutron Source, a DOE Office of Science User Facility operated by the Oak Ridge National Laboratory. The work at ORNL was supported by the U.S. Department of Energy, Office of Science, Office of Basic Energy Sciences, under contract number DE-AC05-00OR22725. The work at the University of Warwick was supported by the EPSRC, UK, through Grant EP/M028771/1. Additional neutron scattering experiments were carried out at the continuous spallation neutron source SINQ at the Paul Scherrer Institut at Villigen PSI in Switzerland.

Author contributions

Project and experiments were designed by R.S., T.F. and M.K. Crystal growth and characterization were performed by R.S., M.C.H. and G.B. Sample alignment and mounting for the neutron scattering experiment was realized by R.S. and N.G. Neutron scattering experiments were carried out by R.S. and N.G. with J.O. and B.W. as local contacts. The experimental data were analyzed by N.G., R.S., T.F. and M.K. Calculations were made by H.Y. and N.S. The paper was written by R.S. with feedback from all authors.

Competing financial interests

The authors declare no competing financial interests.

Methods

Sample preparation

A large single-crystal of $Pr_2Hf_2O_7$ was grown by the floating zone technique using an optical furnace equipped with high-power xenon-arc lamps[31]. The sample was characterized by synchrotron X-ray powder diffraction for a precise determination of the lattice parameter[31]. Additional single-crystal neutron diffraction data were collected on the Zebra instrument, a technique that provides an excellent contrast between the three atoms present in $Pr_2Hf_2O_7$. Attempts to refine antisite cation disorder and oxygen Frenkel disorder, which can induce stuffing effects and disordered interactions and environments, respectively, did not provide evidence for structural defects.

Neutron scattering experiments

The unpolarized inelastic neutron scattering experiment was performed with the IN5 time-of-flight spectrometer at the Institut Laue-Langevin, Grenoble, France[32]. The single crystal, mounted on a copper sample holder and fixed with copper wires, was aligned in the (H,H,L) plane in reciprocal space. Measurements were carried out at a temperature T = 0.05 K with a fixed incident neutron energy E_i = 2.70 meV and an energy resolution of 0.050 meV at zero energy transfer. The measurements were taken while rotating the sample about the vertical axis. The data analysis was performed using HORACE analysis software[33]. The raw data were corrected for time-independent electronic noise, and for neutron absorption by a finite element analysis based on the sample geometry. For the elastic scattering results, measurements at T = 50 K were used for background subtraction. The presented data are symmetrized: they were folded in the first quadrant to improve statistics, unfolded to cover the four quadrants and smoothed.

The polarized inelastic neutron scattering experiment was performed with the HYSPEC time-of-flight spectrometer[34] at the Spallation Neutron Source, Oak Ridge National Laboratory, USA. The same single crystal measured with the IN5 spectrometer was oriented in the (H,H,L) plane in reciprocal space on a copper sample holder and fixed with copper wires. Measurements were carried out at a temperature T = 0.05 K with an incident neutron energy E_i = 3.8 meV. The neutrons were polarized using a Heusler crystal array, and analyzed with the polarization analyzer constituted of a supermirror array designed and built at the Paul Scherrer Institut[34]. A Mezei flipper located between the monochromator and the sample was used to flip the polarization and measure both spin flip and non-spin flip scattering. A multi-coil electromagnet surrounding the sample was used to rotate the incident vertical neutron polarization to a polarization in the horizontal scattering plane. In the standard notation of neutron polarization analysis, the polarization X describes a neutron spin polarized parallel to the momentum transfer **k**, and in these conditions all magnetic scattering events occur through spin-flip scattering. In the reported experiment, the polarization direction in the horizontal plane was fixed to be parallel to the momentum transfer **k**, when it takes a value $|\mathbf{k}| = 1.02$ Å^{-1}. The data reported here are integrated in a small region in reciprocal space around $|\mathbf{k}| = 1.02$ Å^{-1} and therefore represent X-polarized scattering in the standard notation of neutron polarization analysis. Measurements of the sample holder without the sample were used for background subtraction. Data were corrected for the flipping ratio of the neutron spin with measurements of spin flip and non-spin flip scattering of quartz. The mirror-dependent transmission of the supermirror array was calibrated by using

vanadium as a standard. The energy-dependent mirror transmission was also corrected based on previous calibration of the supermirror array.

Fitting of the experimental data to model calculations

The analytical predictions of $S(\boldsymbol{q})$ from Quantum Spin Ice (QSI) in Fig. 1 and Fig. 3 are calculated with the $U(1)$ lattice-gauge theory described in Ref. 5. The $S(\boldsymbol{q})$ from Classical Spin Ice (CSI) model are calculated based on Refs. 5, 35 and 36. The QSI model corresponds to the limit $U \gg W$ in Ref. 5, while the CSI model corresponds to the limit $W \gg U$.

In both Fig. 1 and Fig. 3, the magnetic form factor of Pr^{3+} in the dipolar approximation is included to be consistent with experiments. Furthermore, for Fig. 3, the analytical results are integrated over the same range as the experimental data, which is $(\pm 0.1, \pm 0.15)$ for (H, L) inside (H, H, L) plane, and ± 0.05 perpendicular to it.

In order to fit the experimental data with the QSI model in Fig. 3, we used the speed of artificial light c as a fitting parameter, which depends on microscopic details of the material, and overall rescaling and shift of the intensity due to the arbitrary unit of the intensity and paramagnetic background subtraction of experiments, respectively. The optimal value of c, overall rescaling, and shift were obtained through a weighted least-square fit of $\sum_{i\in \text{ all data points}}\left(I_i^{\text{exp}} - I_i^{\text{thy}}\right)^2 / E_i^2$, where I_i^{exp} is the experimental intensity, I_i^{thy} is the theoretical prediction, and E_i the error associated with each data point. For the symmetrized data points of Fig. 3**b**, we included the difference between two points before symmetrization in order to reflect the fluctuation that caused the asymmetry, which is not counted in the statistical error for each individual point. The final error is $E_{i(j)}^{\text{sym}} = (((\left(I_i - I_j\right)/2)^2 + E_i^2 + E_j^2)^{1/2}$, where $I_{i,j}$ are the unsymmtrized intensities, and $E_{i,j}$ are their individual statistical errors respectively.

The CSI model is fitted in the same way as the QSI model, but with only the overall rescaling and shift as adjustable parameters. The zero-energy slice of neutron scattering for the CSI model corresponds to our analytical calculation of zero temperature, leaving no further adjustable parameters.

The speed of emergent photon obtained by the fitting is $3.6\ m/s$, and bandwidth $0.01\ meV$, meaning that the energy-integrated $S(\boldsymbol{q})$ of the QSI is within experimental resolution and is the proper quantity to use for the fit.

The weighted square sum is 55.8 for QSI and 79.1 for CSI, showing significant improvement of fitting when quantum effects are switched on. The dip in the center of classical prediction shown in Fig. 3**a** is purely a consequence of the integration over experimental resolution, and its overall slope is from the magnetic form factor. Without these effects, the classical prediction would be a constant, independent of the wave-vector, on this cut through reciprocal space, while the quantum theory shows suppressed scattering near the center $(0,0,2)$ and enhanced scattering near $(0,0,1)$ and $(0,0,3)$.

The speed of light c, overall rescaling, and shift obtained through least square fitting of the QSI to the experimental data are then used to produce the analytical results of Figure 1b.

References (methods)

31. Ciomaga-Hatnean, M. *et al.* Single-crystal growth, structure and magnetic properties of $Pr_2Hf_2O_7$ pyrochlore. *J. Phys.: Condens. Matter* **29**, 075902 (2017).

32. Ollivier, J. & Mutka, H. IN5 cold neutron time-of-flight spectrometer, prepared to tackle single crystal spectroscopy. *J. Phys. Soc. Jpn* **80**, SB003 (2011).

33. Ewings, R. A. *et al.* Horace: Software for the analysis of data from single crystal spectroscopy experiments at time-of-flight neutron instruments. *Nucl. Instrum. Methods Phys. Res. Sect. A* **834**, 132–142 (2016).

34. Winn, B. *et al.* Recent progress on HYSPEC, and its polarization analysis capabilities. *EPJ Web of Conferences* **83**, 03017 (2015).

35. S. V. Isakov, K. Gregor, R. Moessner, S. L. Sondhi, *Phys. Rev. Lett.* **93**, 167204 (2004).

36. C. L. Henley, *Phys. Rev. B* **71**, 014424 (2005).